

Visualization of wave-induced suspension patterns over two-dimensional bedforms

PAUL V. VILLARD¹ and PHILIP D. OSBORNE²

Department of Geography, University of Auckland, Auckland, New Zealand

ABSTRACT

High spatial and temporal resolution measurements of suspended sand concentration (c) over vortex ripples were collected with a three-transducer acoustic backscatter sensor (ABS) array, under irregular 'natural' waves in a multidirectional wave basin. These measurements permit two-dimensional visualization of the movement of sediment-laden vortices over an individual vortex ripple under a series of waves. Patterns of sediment motion were tracked through consecutive zero-crossings in the horizontal velocity (U) record measured at 0.05 m above the ripple crest elevation. It was possible to trace the advection of individual sediment-laden vortices at the zero-crossings. During 73% of these events, shedding and advection of coherent suspension events occurred before the flow reversal associated with the zero-crossing. This may be caused by the bedforms retarding the near-bed flow inducing the eddy shedding before the zero-crossing. While at maxima in U , secondary suspension events with low c were observed to pass over the ripple crest moving with U measured at 0.05 m. This pattern is attributed to vortex shedding from adjacent bedforms and/or antecedent suspension events. The most energetic events appeared to persist for several wave cycles and reached heights of ≈ 0.20 m. These suspension events appeared to be more persistent when smaller waves follow larger waves, possibly as a result of weaker reversals in vorticity. Although the events appeared to be vertically coherent in the time series from the individual transducers, it is apparent through visualization that these events are associated with the pairing of antecedent and developing vortices.

Keywords Acoustic backscatter sensor, flume, ripples, sand transport, vortices.

INTRODUCTION

A number of sediment transport models rely on prediction of the time-varying profile of suspended sediment concentration in order to calculate the vertical variation in suspended sediment flux (e.g. Black, 1994; Davies, 1995). However, meas-

urements of the time-varying suspended sediment concentration (c) under waves often exhibit complicated temporal and spatial patterns that are not easily reconciled through simple relationships with the near-bed fluid forcing. A number of measurements obtained using high-resolution acoustic backscatter sensor (ABS) arrays illustrate the difficulty of interpreting the suspension process under waves from measurements that have limited spatial context (e.g. Vincent & Green, 1991; Hay & Bowen, 1994a,b; Villard *et al.*, 2000). Although vertical arrays of optical backscatter sensors and ABS provide improved resolution of the vertical variations in c compared with single

Present addresses: ¹University of British Columbia, Department of Geography, 1984 West Mall, Vancouver, BC, V6T 1Z2, Canada (E-mail: pvillard@geog.ubc.ca).

²Pacific International Engineering, PLLC, PO Box 1599, Edmonds, WA 98020-4121, USA.

point sensors, relatively little attention has been given to resolving the horizontal extent and variability of wave-induced suspension events.

This paper provides an interpretation of episodic wave-induced suspension events based upon detailed high-resolution measurements made with a three-transducer ABS and qualitative visual observations of the measured suspension patterns. A method is presented for quantitative visualization of two-dimensional (vertical and horizontal) patterns of c that involves interpolating the ABS measurements. This method of visualization is found to be useful for investigating the relationships between horizontal velocities, vortex shedding and advection, and helps to clarify the mechanisms producing large, vertically coherent suspension events under wave groups.

WAVE BASIN, INSTRUMENTATION AND EXPERIMENTAL DESIGN

The purpose of the experiment was to examine the evolution of bedforms and associated sand suspension under an irregular wave field (Osborne *et al.*, 1994) at near-prototype scale. The data were collected during an experiment conducted in the multidirectional wave basin at the Institute for Research on the Canadian Environment (Canadian Hydraulics Laboratory, National Research Council) in Ottawa. The dimensions of the multidirectional wave basin are 30 m by 20 m and 3 m deep. The basin is equipped with a 60-segment snake-type wave generator that can produce short-crested, multidirectional seas with waves up to 0.7 m (Davies *et al.*, 1994). A 20-min wave record was synthesized from field measurements collected from the nearshore of Bluewater Beach (BWB), Georgian Bay (Osborne & Greenwood, 1992). Waves were reproduced at a scale of 1:1.8 in a water depth of 1.6 m with an average wave period of 2.7 s. The test section was a 5 m by 5 m area in the centre of the basin covered with a horizontal bed of commercial-grade, well-sorted silica sand having a mean diameter of 0.25 mm (estimated fall velocity $\approx 0.031 \text{ ms}^{-1}$; van Rijn, 1989). The thickness of sand on the test section was graded from 0 to 0.2 m from the down-wave to the up-wave edge, resulting from a slope of 1:25 in the wave basin floor (Osborne *et al.*, 1994).

An array of instruments to measure time series of concentration profiles (c), horizontal velocities (U), water surface elevations and bedform condi-

tions was suspended above the test section from scaffolding. Figure 1 is an idealized schematic diagram of the particular instruments used to collect the data presented in this paper. Suspension patterns were monitored qualitatively with oblique underwater video, while a three-transducer ABS, which operates at frequencies of 1.97 MHz (F1), 4.07 MHz (F2) and 5.57 MHz (F3), produced quantitative measurements of c . The transducers were set 0.65 m above the bed and 0.06 m apart, with F1 situated closest to the wave generator, followed by F2 and F3 in the down-wave direction (Fig. 1). The ABS produces profiles of c with a vertical resolution of 0.005 m. To reduce statistical uncertainty associated with individual concentration estimates, profiles from 12 acoustic returns were averaged during data collection from each transducer to produce profiles of c at a rate of 0.24 s ($\approx 4.2 \text{ Hz}$). Each sampling burst consisted of 2050 profiles ($\approx 8 \text{ min}$). The algorithm outlined by Vincent & Downing (1994) for converting the acoustic backscatter to a sediment concentration is used here. Each of the three transducers was calibrated in the University of East Anglia recirculation tank with sand collected from the wave basin test section.

The video system was used to monitor bedform development and observe the suspension patterns qualitatively. The video field of view was set to monitor the bedforms and suspension patterns occurring below the three transducers (Osborne *et al.*, 1994). The video was manually

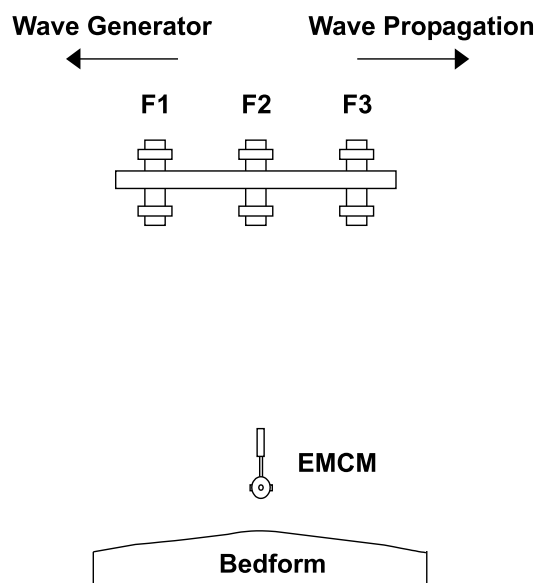


Fig. 1. Configuration of ABS and EMCM; wave propagation was from left to right; diagram is not to scale.

synchronized to within a half second of the ABS collection.

Time series of horizontal velocity (U) were collected from an electromagnetic current meter (EMCM) set at a height of 0.05 m above the bed and in line with transducer F2. The ABS data acquisition system also sampled the EMCM to ensure synchronization between measurements of c and U .

Bedform height and spacing below the transducer array, bed elevation change over time and the position of the ABS transducers relative to the bedforms were monitored visually from above the instrument array and interpreted from direct measurements of bed position from the ABS (Osborne *et al.*, 1994).

Bursts of data were obtained from instrumentation at the end of a 40-min period of wave generation, allowing bedforms to evolve to equilibrium for each set of wave conditions. Results from one of the runs from these experiments are presented here.

BEDFORM GEOMETRY AND POSITION WITH RESPECT TO INSTRUMENTATION

Bedforms were symmetric, linear-crested vortex ripples that had an average length of 0.106 m and an average height of 0.028 m. As instrument position with respect to the bedform influences the temporal and spatial patterns of suspension (e.g. Nielsen, 1992; Osborne & Vincent, 1996), the temporal change in bed position below each transducer was measured. Based on visual observation, it appeared that the bedform did not migrate or shift position in response to the passage of individual waves or wave groups during the wave generation sequence. The elevation of the bed (± 0.005 m) below the three transducers was measured using the ABS. In most profiles of the water column, the bottom location is clearly identified by a sharp peak in the backscatter pressure resulting from sharp changes in the acoustic impedance between the fluid and the bed (Hanes *et al.*, 1988).

Figure 2 illustrates the temporal variation in bed positions measured by the three ABS transducers during the irregular wave series. Each of the bed position series has been smoothed with a 40-point (≈ 10 s) moving average filter to remove large 'apparent' shifts in bed position caused by periodic, energetic sand suspension. Although there is no systematic shift in the bed position under the three transducers over the run, fluctu-

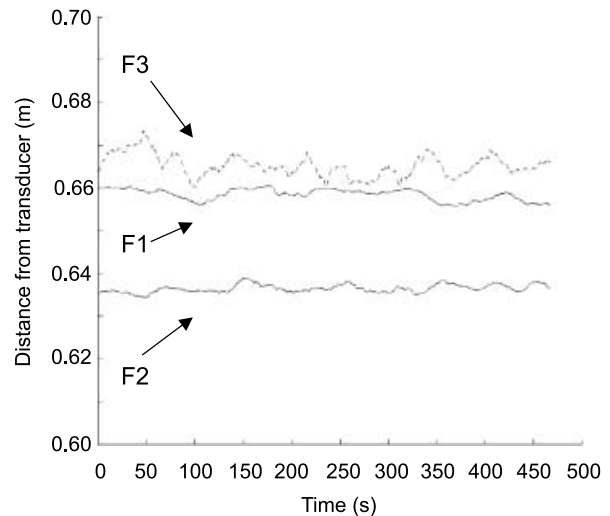


Fig. 2. Time series of the bed positions from transducers F1, F2 and F3.

ations of the order of ≈ 0.01 m in the bed position are evident in the time series and are associated with periods of energetic near-bed suspension. The lack of a long-term change in bed position below the three transducers corresponded with the visual observations, indicating that there was no significant migration or change in either geometry or size of the bedforms during the run. Therefore, the bed platform and profile are treated as stationary throughout the subsequent analysis.

As the vertical resolution of the ABS is limited to ± 0.005 m, it is possible that measurements of c from the lowermost bins of the ABS profile may be contaminated by the presence of the bottom boundary. A persistent feature in almost all the time-averaged profiles is an inflection point near the bed (Vincent & Downing, 1994; Green & Black, 1999), which represents the transition between the bed and the water column in a time-averaged sense. Therefore, the inflection point from the time-averaged c profile is used to define the lower limit for estimates of c to avoid the possibility of any contamination. This method is similar to that used by Green & Black (1999).

Using this definition, the relative positions of the lower limits of the concentration profiles suggest that the profiles below transducer F1 begin 0.025 m lower than at transducer F2, and that the profiles below F3 begin 0.02 m lower than at transducer F2. This corresponds to the visual observations indicating that transducers F1 and F3 were situated near the bedform trough, whereas transducer F2 was near the bedform

crest. This observation indicates a local trough spacing of ≈ 0.12 m.

DESCRIPTION OF RANDOM WAVE FIELD

Time series of both U measured by the EMCM and c measured by the three ABS transducers for ≈ 490 s (2050 points) of the simulated series (Fig. 3) show several patterns. First, peaks in sediment suspension are associated with the wave groups. Second, these energetic suspension events are characterized by peaks in near-bed suspension that are persistent over several wave cycles, with the injection and pumping up of suspended sediments to heights of ≈ 0.20 m. Third, sediment suspension above ≈ 0.10 m appears to lag behind the peaks in near-bed concentration. Finally, no significant suspension appears to occur between the groups of large waves.

Video and visual observations indicate that the suspension was driven by vortex growth and shedding. Visual observations concur with the ABS, in that suspension appeared to occur preferentially under the crests of larger waves and during the passage of wave groups. The

suspension pattern consisted of the discrete shedding of the vortices from the ripple troughs, with visual observations indicating that individual vortices developed in the lee of the ripple crest. Near the zero-crossing, defined as the reversal in the horizontal velocity record, the vortices were ejected and advected horizontally with the instantaneous horizontal velocity. Events appeared to develop and dissipate quickly after shedding, lasting for only one or two wave periods. These visual observations conflict with the ABS measurements, which showed that events were more persistent, lasting up to several wave cycles. The difference between acoustic and visual observations of the persistence of suspension events may be attributed to the sensitivity of the different methods of visualization.

Figure 4 shows time series of U measured by the EMCM and c measured by the three ABS transducers for one wave group, approximately four wave cycles. There appears to be a rapid increase in concentration, which expands up to ≈ 0.20 m. Although there is a high degree of intrawave variability, identifying the systematic patterns within and between transducers is difficult, as presenting the data as a time series

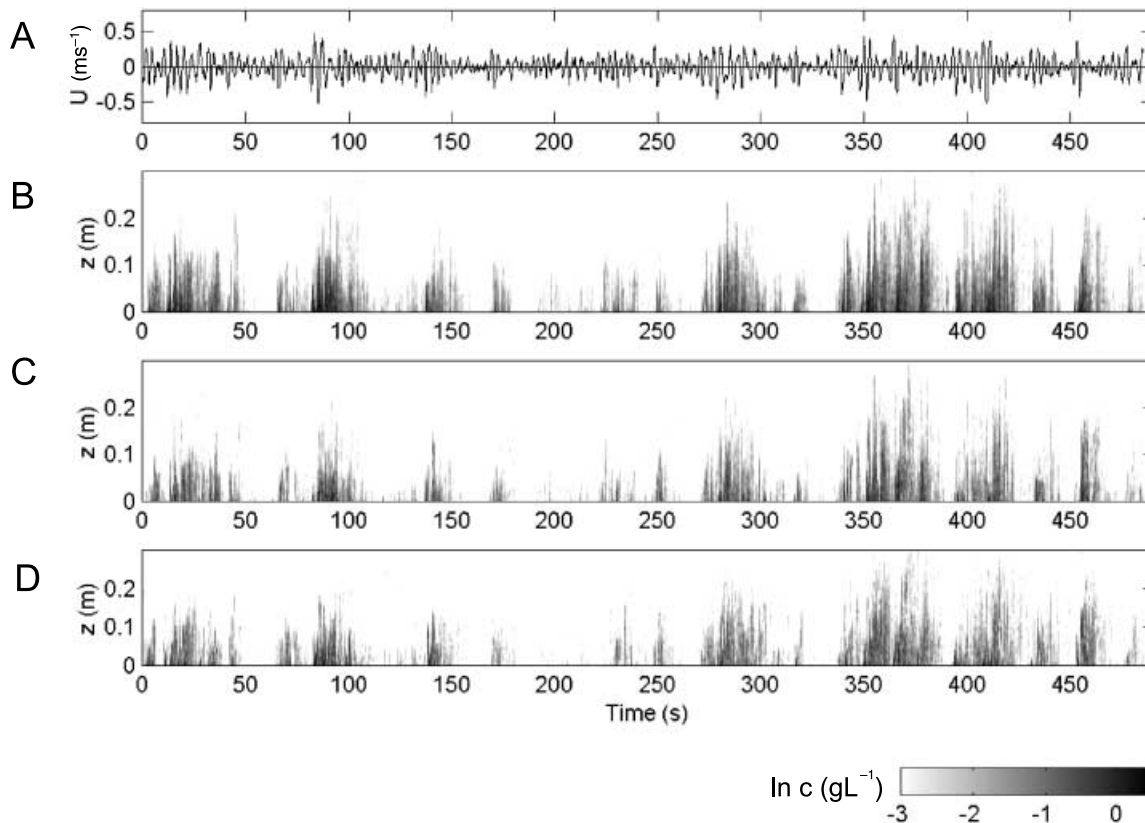


Fig. 3. Time series of horizontal velocity from the EMCM (A) and profiles of logarithm c from the three ABS transducers F1 (B), F2 (C) and F3 (D).

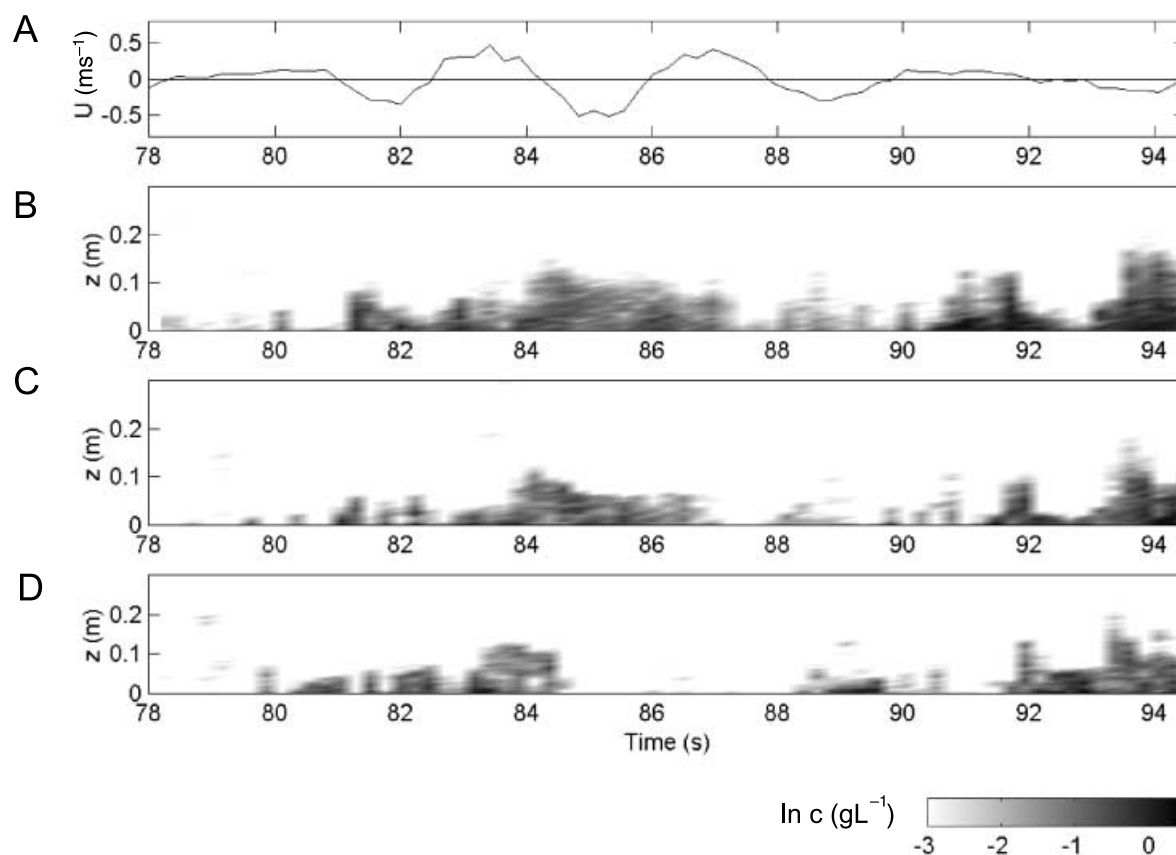


Fig. 4. Time series of horizontal velocity from the EMCM (A) and profiles of logarithm c from the three ABS transducers F1 (B), F2 (C) and F3 (D) for a short segment of the burst.

does not portray the existing spatial relationships clearly.

Cross-correlation was used to examine the vertical extent of a wave group-scale suspension event and relative rate of vertical expansion of the event between 60 and 110 s from the start of the time series (see Fig. 3). A 200-point segment of the time series from the lowest bin was cross-correlated with the time series from all the subsequent bins at higher elevations (Fig. 5). There is a high coherence, with no lag in peak correlation to a height of ≈ 0.15 m. Above this height, the peaks in correlation exhibit a systematic lag, indicating that the event in this segment was migrating vertically over the period of several wave cycles (Fig. 5).

TWO-DIMENSIONAL PATTERNS OF SUSPENDED SEDIMENT OVER A WAVE-FORMED BEDFORM

Visual observations, together with the statistical descriptions from the individual profiles, were compared with the patterns observed from a two-

dimensional, spatial interpolation of c above an individual ripple. The interpolation of a concentration map at each time step from the three ABS transducers provides a picture of the development and migration of sediment-laden vortices over a single bedform. The bedform below the sensor was a simple symmetric linear ripple, with the trough-to-trough distance equivalent to the transducer separation. The ripple crest was below the middle transducer, and the outer transducers were in the deepest part of the ripple troughs. Although this simple geometry leads to a two-dimensional suspension pattern, it also limits the influence of advection of sediment parallel to the wave crest, an important factor once the bedforms become three-dimensional.

Each of the three profiles was referenced in the horizontal direction relative to the first transducer in the direction of wave propagation. The vertical position, z , was referenced to the lowest measurement from the three transducers. The three profiles were used to produce an interpolated grid of c . The concentration map consisted of a 1200-point grid, 0.12 m by 0.25 m, with c -values interpolated at 0.005-m increments. Interpolation

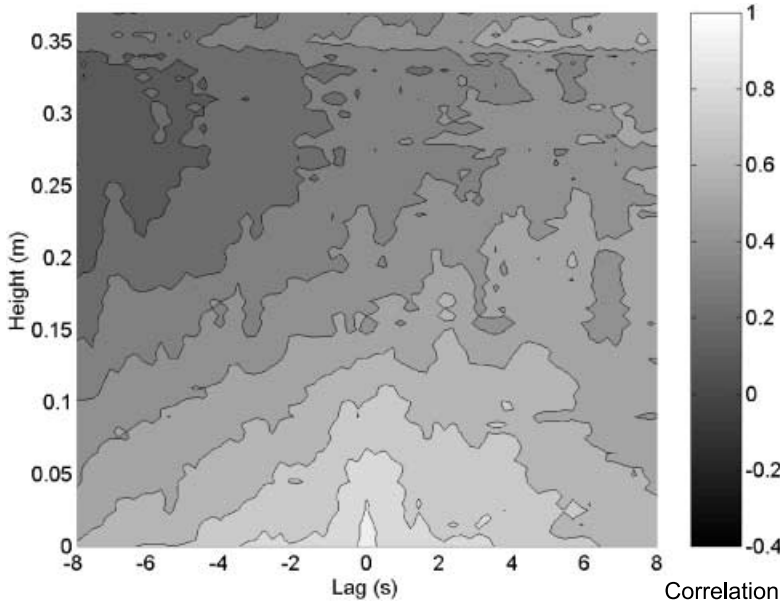


Fig. 5. Surface plot of the variation in normalized cross-correlation with height above the bed from a 200-point segment corresponding to an energetic period of suspension (≈ 62 – 110 s).

was based on the logarithm of c to avoid implausible negative concentrations and to smooth artifact highs and lows produced by the scarce grid of data (Swan & Sandilands, 1995; p. 316). The interpolation was done using the triangular-based nearest neighbour method. This method was chosen because it produces a smooth surface, without the ‘ridges’ and ‘valleys’ produced by interpolating scarce data with more complex quadratic-based algorithms (Swan & Sandilands, 1995; pp. 313–315). Concentrations were converted to g l^{-1} after interpolation for simplicity of interpretation.

Owing to the coarseness of the concentration grid, the ripple form was represented by two back-to-back 90° triangles, with the points below the three transducers defining the co-ordinates of the triangle corners.

Figures 6–10 display a series of concentration maps that step through the four wave cycles illustrated in Fig. 4. Although sequential, intermediate time steps have been left out in some cases to reduce redundancy and condense the time series. Above each concentration map is a plot of the horizontal velocity series, where the ‘*’ indicates the corresponding horizontal velocity and time step. This segment was chosen because it depicts several of the typical intrawave patterns observed through the entire time series. The rapid change in wave forcing also allows the ‘typical’ wave-by-wave patterns observed during the passage of a wave group to be highlighted.

Before the passage of this wave group, there was little suspension because of the passage of

several small waves (Fig. 3). Figure 6A illustrates the low concentration of suspension through the first part of the first wave cycle. During the up-wave (trough)-directed part of the first wave cycle, a localized region of high concentration begins to develop in the leeside trough of the ripple before the peak in horizontal velocity (Fig. 6B and C). The concentration in this region continues to grow with the increase in orbital velocity, while continuing to be confined within approximately one or two ripple heights of the bed. Before the zero up-crossing, the region expands and migrates over the ripple crest, initially travelling in opposition to the instantaneous horizontal velocity measured at 0.05 m (Fig. 6D). As the first event passes out of view on the down-wave side of the ripple, a second event appears on the up-wave side of the ripple and propagates over the ripple with the orbital velocity (Fig. 6E and F). This event probably developed on the up-wave ripple and was then advected with the horizontal velocity.

The pattern observed in the up-wave portion of the wave cycle is mirrored during the down-wave portion (Fig. 7A–D). A high-concentration region begins to develop in the leeside ripple trough near the peak in orbital velocity (Fig. 7A). The event then appears to rise and expand. As the first event grows, a second event in the up-wave trough develops in association with the up-wave ripple (Fig. 7B and C). The down-wave event expands just after the zero-crossing and propagates across the ripple crest and stoss-side ripple trough (Fig. 7D and E). A weaker event higher in

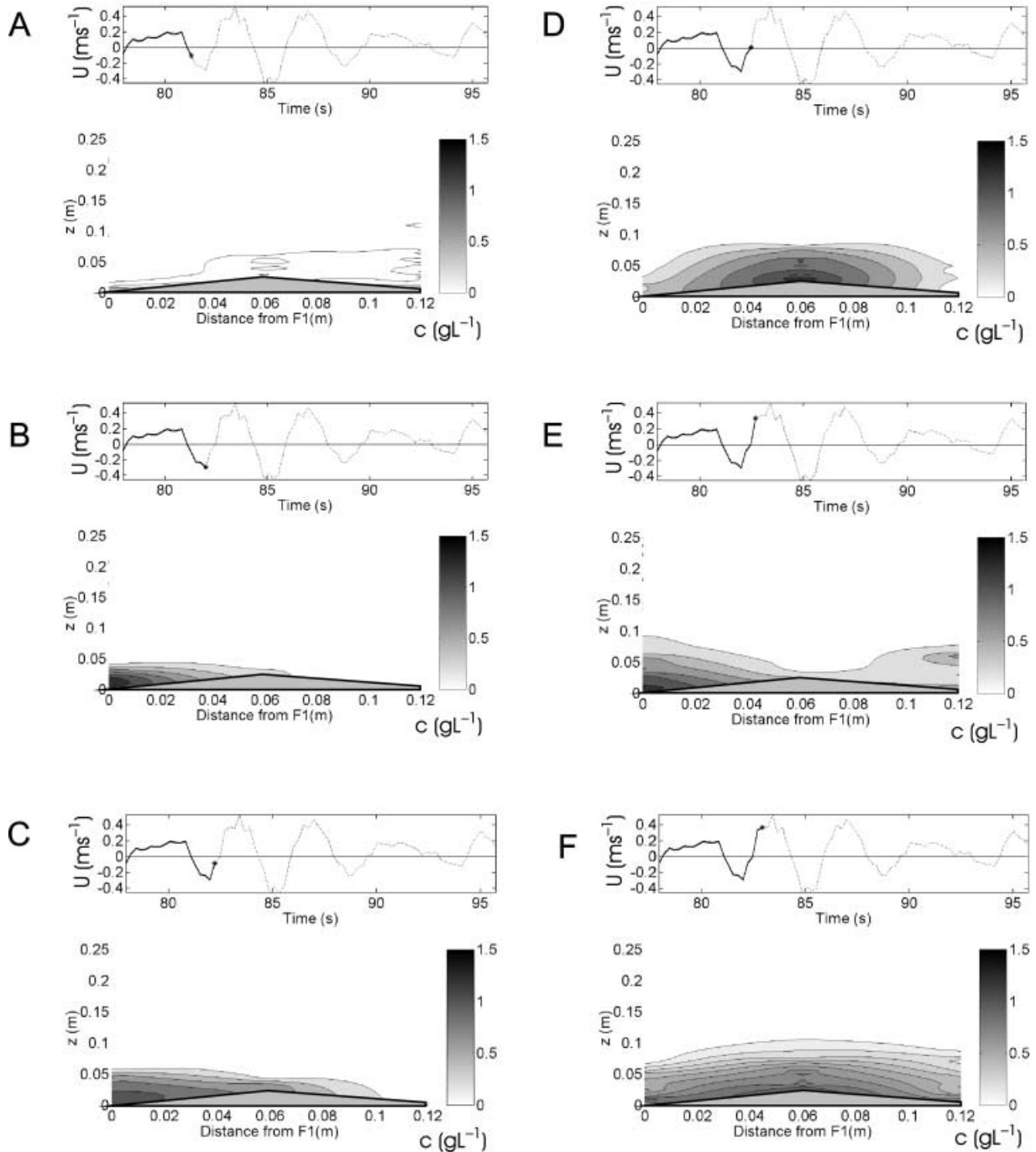


Fig. 6. Maps of c over the bedform corresponding to a series of time steps during a wave group. The horizontal velocity record is plotted above the concentration map, and the asterisk marks the corresponding point in the instantaneous horizontal velocity records. The direction of wave propagation is from left to right in the concentration map. The bedform geometry is approximated by the grey triangle. The vertical exaggeration is 4:8.

the water column (>0.05 m) then appears to migrate from down-wave to up-wave after the shedding of the stronger vortex (Fig. 7F–H).

While the antecedent vortex migrates, a new vortex develops in the trough on the up-wave side of the ripple (Fig. 7F–H). The vertical

extent of the event results from a coupling of the newly developing and the antecedent vortices. This coupling of vortices has been referred to as vortex pairing (Peet & Davies, 1997). The combined event expands and migrates across the ripple crest and down-wave ripple trough

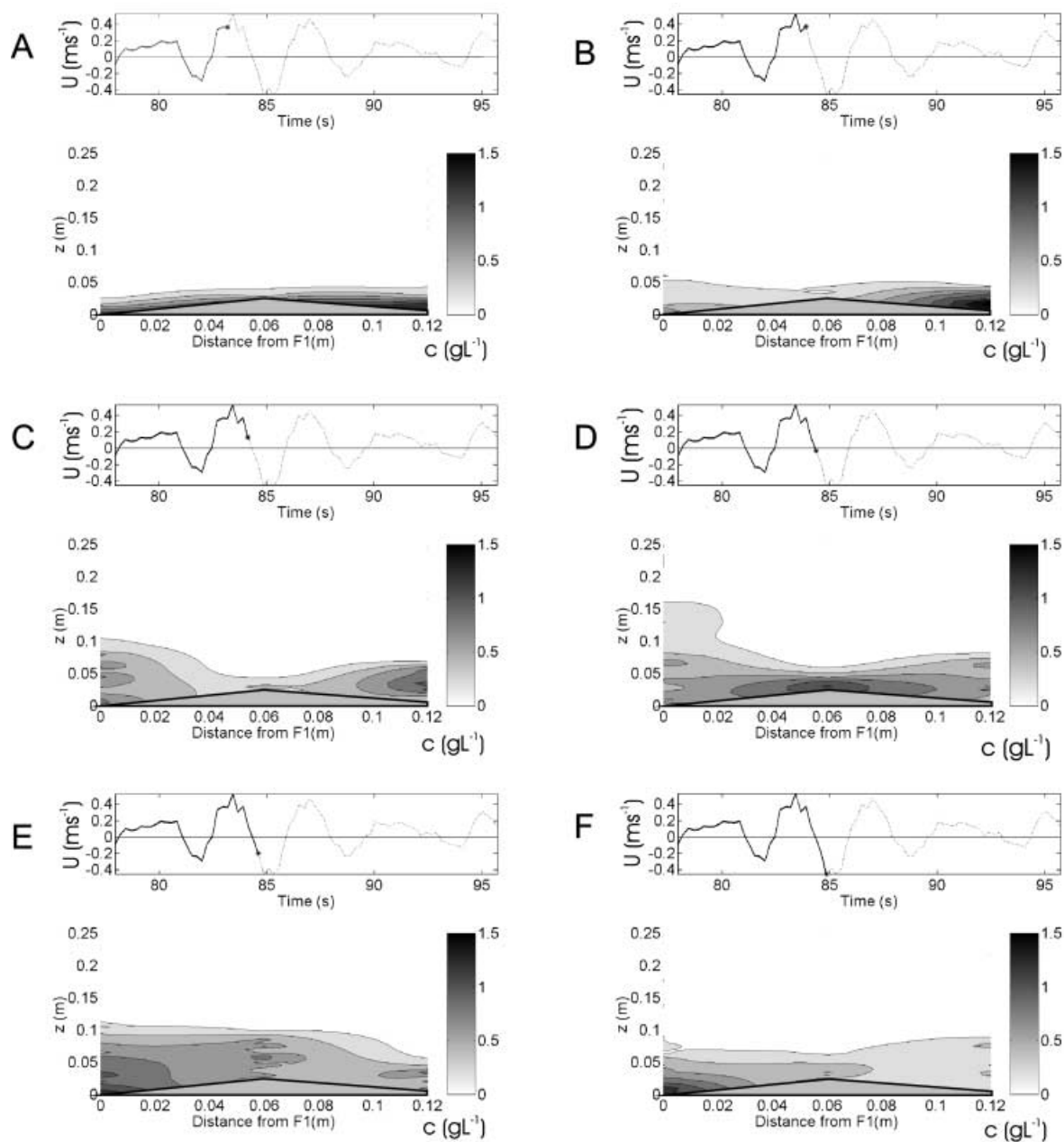


Fig. 7. Maps of c over the bedform corresponding to a series of time steps during a wave group. The horizontal velocity record is plotted above the concentration map, and the asterisk marks the corresponding point in the instantaneous horizontal velocity records. The direction of wave propagation is from left to right in the concentration map. The bedform geometry is approximated by the grey triangle. The vertical exaggeration is 4·8.

(Fig. 7I and J). The patterns that are observed in the first two wave cycles are also evident in the third wave cycle, although the patterns are more difficult to interpret because of antecedent events. Propagation of antecedent suspension events higher in the water column is observed during the passage of this wave (Fig. 8). During the down-wave-directed segment of the third wave cycle, an event (at a height $>0\cdot10$ m)

migrates over the ripple from up-wave to down-wave (Fig. 8A–D). An event (at a height of $\approx 0\cdot10$ m) passes from the down-wave to the up-wave trough during the up-wave portion of the wave cycle (Fig. 9A–C).

Unlike the previous wave cycles, there is no well-defined eddy development and shedding during the passage of the fourth wave (Fig. 10), although the concentration remains much higher

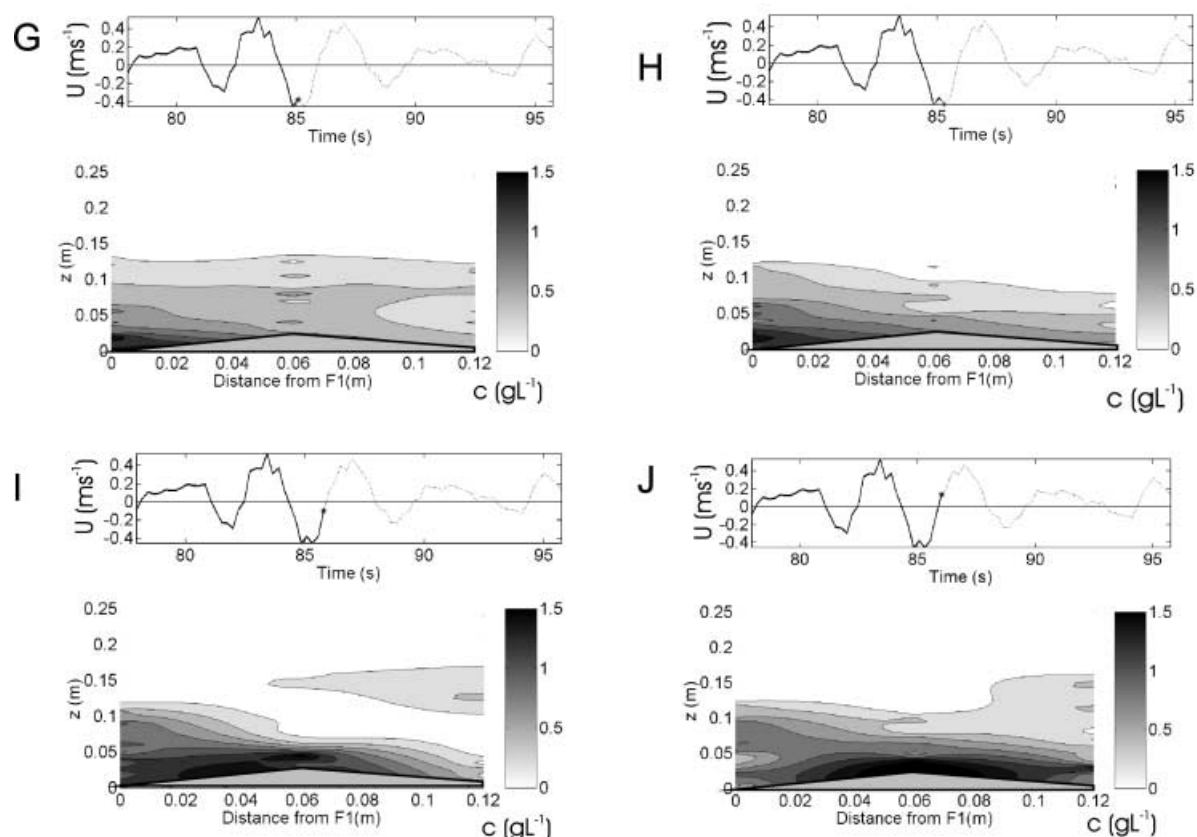


Fig. 7. (Continued).

than that associated with the small wave at the start of the group. Furthermore, the suspension pattern is still heterogeneous throughout the wave cycle, indicating the existence of coherent suspension events, although there is little systematic movement of the high-concentration regions near the bed (Fig. 10A–C). However, the events appear to become more homogeneous and diffuse vertically throughout the last wave cycle. The persistence of the suspended material under the fourth wave appears to be a pattern that develops only when smaller waves follow relatively larger waves.

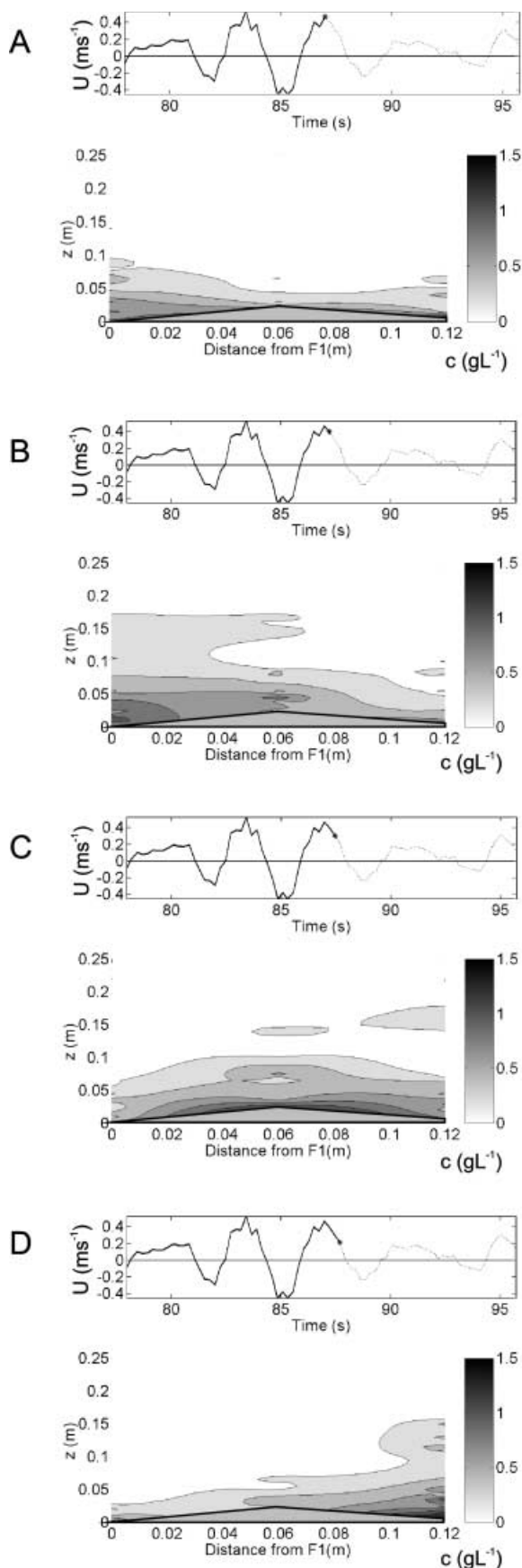
PHASE OF VORTEX SHEDDING AND DIRECTION OF ADVECTION

The movement of individual vortices can be traced by following the development and movement of the regions of high c , even with the relatively sparse spatial and temporal data detailed here. In order to gain a better understanding of the shedding process, the time series of concentration maps was used to relate the

point of vortex shedding and horizontal advection to the instantaneous horizontal velocity measured at 0.05 m.

The entire time series was reviewed on a step-by-step basis and as an animated series (see *Supplementary material*). The animation allowed the direction of transport to be judged, whereas the step-by-step review revealed the timing of events relative to the phase of the zero-crossings in the horizontal velocity measured at 0.05 m. The patterns that occurred around the zero-crossing were broadly categorized as non-events, weak events, shedding-advection events or expansion-advection events. For each wave, the significant horizontal velocity for both the up-wave and the down-wave component was calculated. The significant horizontal velocity, U_{sig} , is defined as the average of the highest one-third absolute instantaneous horizontal velocities measured from each half wave cycle.

The average significant velocity for non-events was 0.16 ms⁻¹ standard deviation ($\sigma_{\text{usig}} = 0.07$ ms⁻¹), much lower than the averages calculated for the three event types. Generally, the



pattern of suspension under waves of this size was characterized by either low homogeneous c or settling, without a systematic movement of regions of high c from transducer to transducer. In some cases, the development of new events was not distinguished because of background suspension occurring when a small wave preceded larger waves that produced relatively high c . From the 299 zero-crossings examined, non-events occurred at 175 zero-crossings (59%). The proportion of non-events concurred with the visual observations that showed energetic suspension associated only with the largest waves and wave groups. This does not mean that vortex shedding was absent during these periods, but that vortices could not be detected by video or ABS on account of the low c associated with the events.

Events classified into the latter three categories were identified at 124 zero-crossings, with 66 occurring at up-crossings and 58 occurring at down-crossings (Table 1). Figure 11 is an idealized sequence of events for each of the three categories of suspension events. The idealized sequences are based on patterns associated with the zero up-crossing and were mirrored during the zero down-crossing. Owing to the relatively slow sampling rate and subjective nature of the analysis, the shedding was classified as occurring before or after the zero-crossing instead of calculating the absolute phase. The most energetic suspension events were labelled as expansion-advection events, with 15 leading and five lagging the point of zero-crossing (Fig. 11A). These events are characterized by the development of a zone of high concentration in the leeside near the peak in horizontal velocity (i). The event expands from the trough to the crest, without a significant decrease in c in the trough (ii). In 80% of the expansion-advection events, the vortex expands across the ripple crest before the zero-crossing, in opposition to the near-bed instantaneous horizontal velocity at 0.05 m. The event then migrates down-flow and out of the field of view (iii). Migration from the ripple crest to the

Fig. 8. Maps of c over the bedform corresponding to a series of time steps during a wave group. The horizontal velocity record is plotted above the concentration map, and the asterisk marks the corresponding point in the instantaneous horizontal velocity records. The direction of wave propagation is from left to right in the concentration map. The bedform geometry is approximated by the grey triangle. The vertical exaggeration is 4.8.

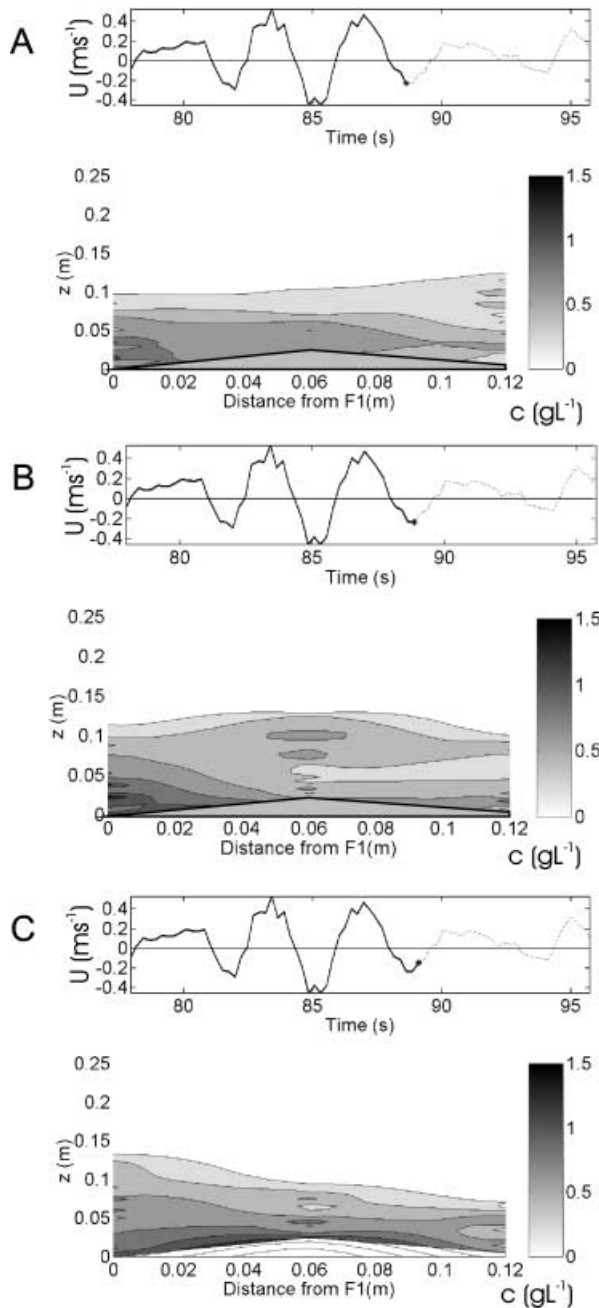


Fig. 9. Maps of c over the bedform corresponding to a series of time steps during a wave group. The horizontal velocity record is plotted above the concentration map, and the asterisk marks the corresponding point in the instantaneous horizontal velocity records. The direction of wave propagation is from left to right in the concentration map. The bedform geometry is approximated by the grey triangle. The vertical exaggeration is 4·8.

down-flow transducer was usually associated with a sudden decrease in c at the crest. The mean significant orbital velocity for these events was $0·31 \text{ ms}^{-1}$ ($\sigma_{\text{usig}} = 0·08 \text{ ms}^{-1}$).

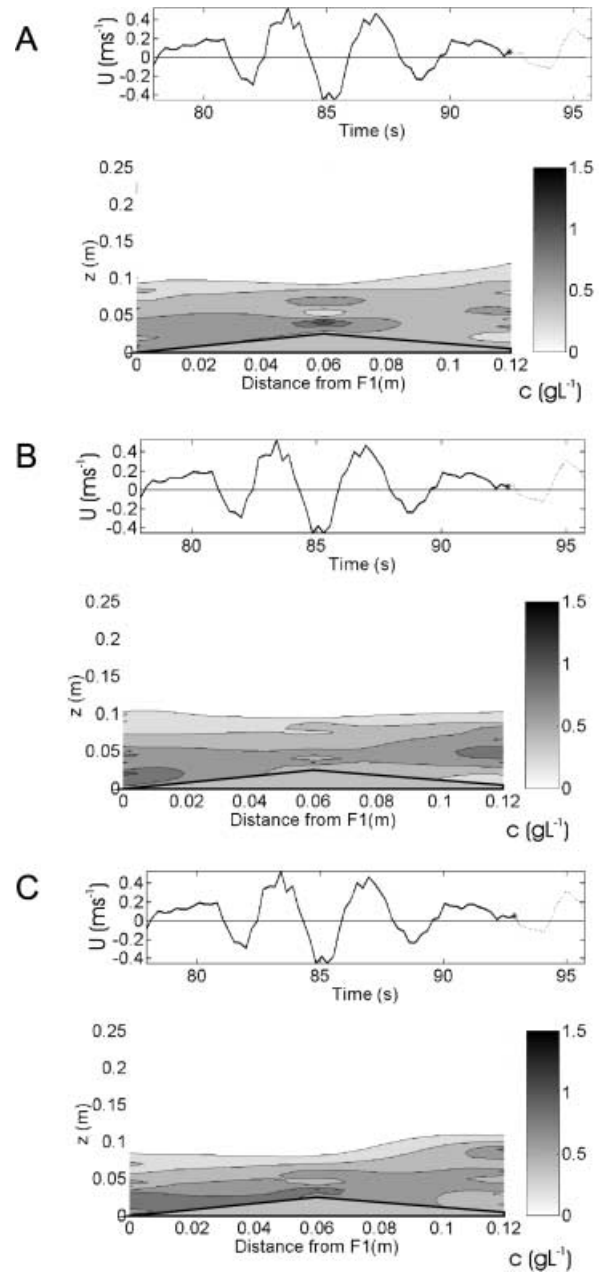


Fig. 10. Maps of c over the bedform corresponding to a series of time steps during a wave group. The horizontal velocity record is plotted above the concentration map, and the asterisk marks the corresponding point in the instantaneous horizontal velocity records. The direction of wave propagation is from left to right in the concentration map. The bedform geometry is approximated by the grey triangle. The vertical exaggeration is 4·8.

The shedding-advection pattern was observed at 61 zero-crossings and had an average significant velocity of $0·28 \text{ ms}^{-1}$ ($\sigma_{\text{usig}} = 0·08 \text{ ms}^{-1}$), slightly lower than those associated with expansion-shedding events (Fig. 11B). The

Type of event	Lead zero-crossing	Lag zero-crossing
Expansion-advection	15 (12.1%) (<i>12/3</i>)	5 (4.0%) (<i>0/5</i>)
Shedding-advection	45 (36.3%) (<i>27/18</i>)	16 (12.9%) (<i>3/13</i>)
Weak event	30 (24.2%) (<i>24/6</i>)	13 (10.5%) (<i>0/13</i>)

Bold values in brackets are a percentage of the total number of events, and italicized values in brackets are the absolute numbers occurring at up-crossings and down-crossings.

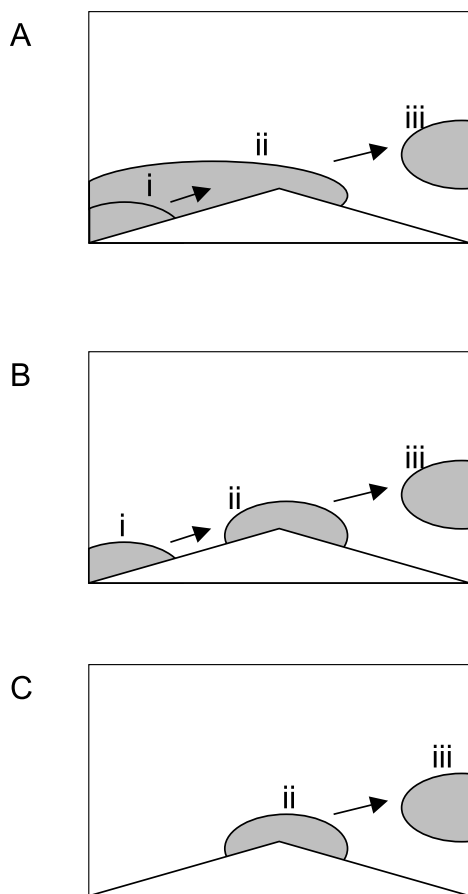


Fig. 11. Idealized representation of the three categories of event sequences observed at zero-crossing, expansion-advection (A), shedding-advection (B) and weak shedding (C).

event is initiated after the peak in velocity in the up-wave or down-wave trough (i). The event then propagates across the ripple crest (ii). A rapid decline in c in the trough is associated with the event appearing at the crest. In 16 (12.9%) cases, shedding and horizontal advection of the event lagged the zero-crossing, whereas in 45 (36.3%) cases, shedding and advection of the event led the zero-crossing. The event then moves with the flow, through the downstream transducer and out of the field

of view. Again, the advection of the suspension event corresponds with a rapid drop in c at the adjacent down-flow transducer (the crest) (iii). This pattern is not unusual and corresponds to both the pattern described qualitatively by other authors (e.g. Bagnold, 1946; Sunamura, 1980; Sleath, 1982) and the visual observations described here.

It appears that more of the events that lag the zero-crossing occur on the zero down-crossing. This is probably a product of the positioning of the transducers with respect to the crest and troughs. As there are only three transducers, a slight misalignment of the transducers with respect to the bedform will have an effect on the observed timing of events. Even with this variation resulting from positioning, the majority of the events lead the zero-crossing during both down- and up-crossings.

Owing to the limited spatial resolution of the ABS, the high bedload transport observed by other authors above the ripple crest under the wave crest and trough was not observed. The shedding-advection pattern also indicates that the horizontal excursion lengths between time steps are less than the distance between transducers. In order to test that this is reasonable, the significant horizontal velocity, 0.25 ms^{-1} (defined as the average of the top one-third of velocities for the down-wave cycle from the velocity record), is multiplied by the sampling rate to produce a significant advection distance between samples of 0.06 m . Therefore, under all but the peak velocities, the excursion is less than the distance between transducers.

Under some of the smaller waves, the initial high values of c in the trough did not occur. Instead, just before or after the zero-crossing, a zone of relatively high values of c appeared at the crest (ii) and then moved through the down-flow transducer (iii) (Fig. 11C). The average significant velocity was 0.23 ms^{-1} ($\sigma_{\text{usig}} = 0.07 \text{ ms}^{-1}$). In 13 (10.5%) cases, shedding and advection lagged the zero-crossing, whereas in 30 (24.2%) cases,

Table 1. Number of events in each category.

shedding and horizontal advection of the event led the zero-crossing.

If all three categories of events are examined collectively, it is noted that, in 73% of the zero-crossings, the shedding and advection of the event leads the zero-crossing. If the events that can only be followed from initiation to advection are considered, the shedding and horizontal advection leads the zero-crossing in 74% of cases. This indicates that, in the majority of events observed, the sediment-laden vortex moved initially in the opposite direction to the instantaneous horizontal velocity measured at 0.05 m. Furthermore, immediately after all the shedding-advection and expansion-advection events, a second lower concentration event propagated from trough to crest to trough approximately in phase with the peak velocity and moved in the direction of the horizontal velocity. This second peak was not generally found to occur after the passage of the weaker eddy.

DISCUSSION

Some of the small-scale variability in c measured by the ABS arises from the inherent noise produced by the random phase shift associated with the ensemble of returns from individual particles (Hay, 1983; Thorne *et al.*, 1991; Hay & Bowen, 1994a,b). Hay & Bowen (1994b) measured correlation strength vertically and horizontally to illustrate that the intrawave variability was associated with coherent suspension events and was not inherent in the ABS. The visual observations and patterns apparent in the time series of concentration maps in the present study illustrate qualitatively that variability observed in the time series is attributed to the development, shedding and migration of sediment-laden vortices. The concentration patterns observed fit both the visual observations and the conceptual models of vortex shedding presented by other authors (e.g. Bagnold, 1946; Sunamura, 1980; Sleath, 1982; Crawford & Hay, 1995).

Several authors have identified systematic intrawave variability in c through ensemble averaging (phase averaging) of concentration time series. However, the phase relationships and number of peaks in c within wave cycles vary considerably (e.g. Vincent & Green, 1991; Osborne & Vincent, 1996; Nakato *et al.*, 1977; Villaret & Davies, 1997). The variability in phase relations between velocity and concentration is

easily explained by the position of the sensor relative to the bedform, as highlighted by the observations presented here. Variability in the number of peaks observed by different authors can also be explained from the observations presented here. The ratio of weak to strong eddies accounts for the variability in the number of peaks within the wave cycle. It was observed that, under small waves, the events from neighbouring bedforms did not survive to pass over the adjacent bedform. Under more energetic conditions, a second set of suspension events associated with peaks in orbital velocity was apparent. This argument is supported by the ensemble averaging presented by Vincent & Green (1991; their figs 2 and 3), which illustrates that, depending on the magnitude of the wave forcing, either two or four peaks in suspension are apparent in the ensemble-averaged suspension patterns. Ensemble averaging may also produce misleading representations of the complexity of the patterns and the variability between waves, as it does not account for the varying importance of antecedent suspension from wave-to-wave (Villard *et al.*, 2000). Based on the observations presented here, it appears that the patterns under each wave cycle are similar; however, the introduction of antecedent suspension makes the suspension pattern under each wave unique (Villard *et al.*, 2000).

Interestingly, the only contradiction observed between the visual observations and the ABS was that the ABS indicated a longer life span and vertical extent of the vortices. Crawford & Hay (1995) showed from their video analysis of sediment suspension over ripples that vortices produced under similar wave conditions only survived through a single wave cycle. Figures 6–10 do not indicate this trend, as little material was entrained during the first wave, and it is likely that little new material was entrained during the passage of the last wave in the group. Moreover, there are still heterogeneous regions of high c ($>1 \text{ g l}^{-1}$) during the wave cycle that reach heights of 0.10 m while passing over the ripple. As the estimated settling velocity of the material is $\approx 0.03 \text{ ms}^{-1}$, it would be expected that much of the material would have fallen out of suspension within one wave period. However, this is not the case, and it appears that material continues to rise throughout the passage of the wave. This implies that not only do these events last through a single wave cycle, but they may persist and remain coherent over several wave cycles, particularly when the waves that produce energetic suspension are followed by relatively smaller waves,

such as in the case of a passing wave group. This is better illustrated in the time series presented in Figs 3 and 4, rather than in the time steps in Figs 7–10.

Two possible explanations for the discrepancy between the visual observations presented by other authors, in particular those presented by Crawford & Hay (1995), and those obtained from the ABS are related to the difference in sensitivity between the two methods. The first explanation is illustrated by estimating equivalent number of grains cm^{-3} for different concentrations. Using the mean diameter of the bed material and a density of 2650 kg m^{-3} , 2 g l^{-1} equates to $\approx 92 \text{ grains cm}^{-3}$, whereas 0.2 g l^{-1} is \approx nine grains cm^{-3} and 0.05 g l^{-1} is equivalent to \approx two grains cm^{-3} . With such low grain counts in the low c events, it is probable that visual observation from video tends significantly to underestimate the duration of events. The ABS is more capable of discerning antecedent vortices with low c than other visualization methods.

The second possible cause relates to the difference in wave conditions presented in this work and in previous studies. In all the previous visual observations, other than those presented by Crawford & Hay (1995), the waves were monochromatic. In this case, the reversal in the velocity gradient and vorticity at the zero-crossing not only release the eddy but begin to dampen the turbulence. During the passage of monochromatic waves, the uniform wave forcing causes eddies to be broken down quickly as a result of the balance between the forces that develop and dissipate the individual eddies. Under a random wave field, the vortices conceivably have more varied life spans dependent on the initial wave forcing that develops the eddy and the forcing associated with the subsequent waves that dissipate it (Villard *et al.*, 2000).

Several authors have noted that suspension events appear to be vertically coherent to several tens of centimetres under wave groups (e.g. Hanes & Huntley, 1986; Osborne & Greenwood, 1993; Hay & Bowen, 1994a,b). Hay & Bowen (1994a,b) argued that the vertical extent of these events made them difficult to relate to the small local bedforms and were therefore related to turbulence from the frame supporting the instruments or unobserved larger bedforms. The visualization presented here indicates that the events with the largest vertical extent are associated with the matching of antecedent and developing vortices. The visualization illustrates that suspension events remained coherent for several wave cycles

(see Figs 6–10) and reached heights of $\approx 0.20 \text{ m}$. Examination of the concentration maps reveals that the large events represent the interaction between new or developing events near the bed and antecedent events higher in the water column. A hypothesis of vortex interaction has been proposed by several authors, but could not be substantiated by visualization (e.g. Hanes & Huntley, 1986; Hay & Bowen, 1994a). Hay & Bowen (1994a,b) noted coherence in suspension events to heights of 0.30 m over bedforms of similar height to those presented here. They did not attribute these events to the local bedforms because of the large vertical extent of the suspension and lack of visual observations. The difference in height of the suspension events observed by Hay & Bowen (1994a,b) and those portrayed here are attributable to the difference in the magnitude of wave forcing. These combined events tend to appear vertically coherent because of the similar phase of new vortex development and the passage of the antecedent vortices over the ripple trough. Sleath (1982) also observed this pattern of suspension enhancement resulting from the coupling of vortices.

Hydrodynamic measurements by Marin & B elorgey (1993) from laboratory experiments support the argument of synchronized horizontal advection of antecedent and developing vortices. Their observations showed a spatially heterogeneous pattern of vorticity and turbulent kinetic energy (TKE) across the ripple, with vertical bands of high TKE migrating across the ripple. A distinct reversal in vorticity occurs approximately half way up these bands, indicating the presence of two distinct vortices produced during the different halves of the wave cycle. These measurements support the observations presented here of pairing of antecedent and developing vortices that may enhance sediment suspension. Recent model results indicate that paired vortices produce higher mixing than single vortex models (Peet & Davies, 1997).

At an intrawave scale, it was found that at least 73% of the total events observed appeared to be ejected and advected across the ripple crest before the flow reversal. This suggests that, in the majority of events, the movement of the vortices initially opposed the direction of the instantaneous horizontal velocity measured at 0.05 m above the bed, indicating that the horizontal velocity nearer to the bed leads the velocity at 0.05 m . It is therefore proposed that the return flow associated with flow separation and retardation of the near-bed flow by the bedforms enables the vortex to

lead the velocity higher above the bed. However, substantiation of this hypothesis requires high-resolution measurements of suspension and velocity over bedforms.

CONCLUSIONS

The interaction of localized, antecedent and advected sediment-laden vortices was examined with two-dimensional visualization of suspended sediment concentration. The time series of concentration maps illustrates the familiar shedding and advection pattern described in numerous, previous visual observations but with the advantage of providing a quantitative estimate of the magnitude and spatial distribution of suspended sediment concentration. Maximum concentration generally occurs in ripple troughs associated with peaks in horizontal velocity, whereas maximum concentration at the ripple crest lags behind the peaks in the trough and is related to advection of coherent suspension events. An understanding of the horizontal context is critical to interpret correctly the relationships between near-bed suspension, suspension higher in the water column and freestream horizontal velocity.

Coherent suspension events were observed between spatially separated transducers of an ABS system. The most energetic suspension events persisted over several wave cycles and reached heights of 0.15–0.20 m. Moreover, suspension events appear to be more persistent when smaller waves follow larger waves. This is attributed to the weaker reversal in the velocity gradient and vorticity that would weaken and break up eddies. Additionally, it was found that the large vertical extent of suspension events observed in one-dimensional profiles by other authors was the result of the combination of antecedent and developing vortices.

Shedding and advection of vortices was identified as leading the reversal in horizontal velocity measured at 0.05 m in 73% of the total observed events. This indicates that the horizontal movement of the vortices is initially in opposition to the horizontal velocity measured at 0.05 m. There are two possible mechanisms driving this pattern. First, the enhanced friction caused by the bedform retards the near-bed flow and, therefore, the near-bed flow leads the flow reversal. Second, the presence of the return flow produced by the flow separation upstream of the crest drives the early shedding of the vortex. High-resolution velocity and sediment suspen-

sion measurements are needed to understand better the influence of individual and paired vortices in sediment transport under wave groups.

ACKNOWLEDGEMENTS

The wave flume research was made possible by support from the engineering and technical staff at the Institute for Research on the Canadian Environment (Canadian Hydraulics Laboratory, National Research Council), Ottawa, Canada. P.V. was supported by a Commonwealth postgraduate scholarship. The work would not have been possible without the computing facilities of the Spatial Analysis Laboratory (Department of Geography, University of Auckland, New Zealand).

SUPPLEMENTARY MATERIAL

Interactive online versions of segments of the time series discussed in this paper can found at the following web address:

<http://www.blackwell-science.com/products/journals/suppmat/SED/SED448/SED448sm.htm>

REFERENCES

- Bagnold, R.A.** (1946) Motion of waves in shallow water: interaction between waves and sand bottoms. *Proc. Royal Soc. London Series A*, **187**, 1–15.
- Black, K.P.** (1994) Suspended sediment load during an asymmetric wave cycle over a plane bed. *Coastal Eng.*, **23**, 95–114.
- Crawford, A.** and **Hay, A.E.** (1995) Spatial distribution of sediment suspension under wave groups. *Proceedings of the Canadian Coastal Conference*. Dartmouth, Nova Scotia, pp. 187–197.
- Davies, A.G.** (1995) Effects of unsteadiness on the suspended sediment flux in co-linear wave-current flow. *Continental Shelf Res.*, **15**, 949–979.
- Davies, M.H., Laurich, P.H., Mansard, E.P.D.** and **Miles, M.D.** (1994) A new wave research flume at NRC. *Proceedings of the International Symposium on Waves and Numerical Modelling*. IAHR, Vancouver, Canada, pp. 166–174.
- Green, M.O.** and **Black, K.P.** (1999) Suspended-sediment reference concentration under waves: field observations and critical analysis of two predictive models. *Coastal Eng.*, **38**, 115–141.
- Hanes, D.M.** and **Huntley, D.A.** (1986) Continuous measurements of suspended sand concentration in a wave dominated nearshore environment. *Continental Shelf Res.*, **6**, 585–596.
- Hanes, D.M., Vincent, C.E., Huntley, D.A.** and **Clarke, T.L.** (1988) Acoustic measurements of suspended sand concentration in the C²S² experiment at Stanhope Lane, Prince Edward Island. *Mar. Geol.*, **81**, 185–196.

- Hay, A.E.** (1983) On the remote acoustic detection of suspended sediment at long wavelengths. *J. Geophys. Res.*, **88** (C12), 7525–7542.
- Hay, A.E. and Bowen, A.J.** (1994a) Coherent scales of wave-induced suspended sand concentration fluctuations. *J. Geophys. Res.*, **99** (C6), 12749–12765.
- Hay, A.E. and Bowen, A.J.** (1994b) Space-time variability of sediment suspension in the nearshore zone. In: *Coastal Dynamics '94, Proceedings of an International Conference on the Role of the Large Scale Experiments in Coastal Research* (Eds A.S. Arcilla, M.J.F. Stive and N.C. Kraus), pp. 962–975. ASCE, New York.
- Marin, F. and B elorgey, M.** (1993) Flow regime and eddy structures into boundary layer generated by the swell above a rippled bed. In: *Euromech 310: Sediment Transport Mechanisms in Coastal Environments and Rivers* (Eds M. B elorgey, R.D. Rajaona and J.F.A. Sleath), pp. 231–245. World Scientific, Singapore.
- Nakato, T., Locher, F.A., Glover, J.R. and Kennedy, J.F.** (1977) Wave entrainment of sediment from rippled beds. *J. Waterw. Port Coast. Ocean Eng.*, **103**, 83–99.
- Nielsen, P.** (1992) *Coastal Bottom Boundary Layers and Sediment Transport*. World Scientific, Singapore, 324 pp.
- Osborne, P.D. and Greenwood, B.** (1992) Frequency dependent cross-shore suspended sediment transport. 1: a non-barred shoreface. *Mar. Geol.*, **106**, 1–24.
- Osborne, P.D. and Greenwood, B.** (1993) Sediment suspension under waves and currents: time-scales and vertical structure. *Sedimentology*, **40**, 599–622.
- Osborne, P.D. and Vincent, C.E.** (1996) Vertical and horizontal structure in suspended sand concentrations and wave induced fluxes over bedforms. *Mar. Geol.*, **131**, 195–208.
- Osborne, P.D., Vincent, C., Greenwood, B., Marsh, S., Webb, M., Boldy, C., Jagger, K. and Zhiming, X.** (1994) Sediment suspension and transport under irregular waves: roughness control on the re-suspension and transport of sediment. *International Symposium: Waves – Physical and Numerical Modelling*. IAHR, Vancouver, Canada, pp. 1617–1626.
- Peet, A. and Davies, A.** (1997) Convection and diffusion of sediment under large waves. In: *Coastal Dynamics '97* (Ed. E.B. Thornton), pp. 28–37. ASCE, New York.
- van Rijn, L.C.** (1989) *Handbook on Sediment Transport by Currents and Waves*. Report H461. Delft Hydraulics, The Netherlands.
- Sleath, J.F.A.** (1982) The suspension of sand by waves. *J. Hydraul. Res.*, **20**, 439–452.
- Sunamura, T.** (1980) A laboratory study of offshore transport of sediment and a model for eroding beaches. *Proceedings of the 17th Coastal Engineering Conference*. ASCE, Sydney, Australia, pp. 1051–1070.
- Swan, A.R.H. and Sandilands, M.** (1995) *Introduction to Geological Analysis*. Blackwell Science, Oxford, 446 pp.
- Thorne, P.D., Vincent, C.E., Hardcastle, P.J., Rehman, S. and Pearson, N.** (1991) Measuring suspended sediment concentrations using acoustic backscatter devices. *Mar. Geol.*, **98**, 7–16.
- Villard, P.V., Osborne, P.D. and Vincent, C.E.** (2000) Influence of wave groups on SSC patterns over vortex ripples. *Continental Shelf Res.* **20**, 2391–2410.
- Villaret, C. and Davies, A.G.** (1997) Effect of bed roughness on net sediment transport by asymmetrical waves. In: *Coastal Dynamics '97* (Ed. by E. B. Thornton), pp. 235–244. ASCE.
- Vincent, C.E. and Downing, A.J.** (1994) Variability of suspended sand concentrations, transport and eddy diffusivity under non-breaking waves on the shore face. *Cont. Shelf Res.*, **14**, 223–250.
- Vincent, C.E. and Green, M.O.** (1991) Patterns of suspended sand. *Euromech 262: Sand Transport in Rivers, Estuaries and the Sea* (Eds R.L. Soulsby and R. Bettress), pp. 117–123. Balkema, Rotterdam.

*Manuscript received 30 October 2000;
revision accepted 29 October 2001.*